Environment Protection Engineering

Vol. 46 2020 No. 3

DOI: 10.37190/epe200303

CHEN CHEN[1] TING CHENG[2], XIAO ZHANG[3], MINTE ZHANG[4], RUIYANG LV[1]

SURFACE MODIFICATION OF FLY ASH SPHEROIDAL PARTICLES AND THEIR APPLICATION IN THE ADSORPTION OF PHOSPHORUS AND CHROMIUM(VI) FROM SINGLE AND COMPETITIVE SOLUTE SYSTEMS

This work focuses on the surface modification of fly ash spheroidal particles and their application in phosphorus and chromium(VI) adsorption. The results show that through surface modification, amorphous silica-alumina gels precipitated on the spheroidal particle surface (by which the microsurface area of the reaction products is effectively enlarged) and the surface zeta potential was changed to fit for adsorbing anions. During the adsorption experiment (single and competitive solute systems), chromium(VI) was easier to adsorb. The surface zeta potential and the existence of competitive ions should be recognized as two important factors affecting adsorption efficiency. A higher temperature could improve the adsorption efficiencies of the two solute systems. The fitting results of the pseudo-second-order model (single and competitive solute systems) show better agreement than those of the pseudo-first-order model at every temperature. The Langmuir adsorption isotherm equation can better simulate the adsorption process in single solute sy039stems, but only the chromium(VI) adsorption process can be fitted by the competitive Langmuir adsorption isotherm in competitive solute systems.

1. INTRODUCTION

As a result of rapid economic development, China currently faces serious wastewater pollution. According to the *National Environmental Statistics Bulletin*, in 2014, China discharged approximately 7.162×10^{10} t of wastewater, of which 2.053×10^{10} t was industrial wastewater and the remainder was domestic sewage [1]. It is well known that major

[1]School of Environmental and Chemical Engineering, Jiangsu University of Science and Technology, Zhenjiang 212005, China, corresponding author, e-mail: chencjust@sina.com

[2]Department of City Science, Jiangsu City Vocational College, Nanjing 210036, China.

[3]Nanjing University and Yancheng Academy of Environmental Technology and Engineering, Yancheng 224000, China.

[4]School of Deep Blue, Jiangsu University of Science and Technology, Zhenjiang 212018, China.

pollutants in wastewater such as phosphorus and chromium(VI) can present severe threats to human health and environmental safety. Many human industrial, agricultural, and domestic activities can discharge phosphorus and chromium(VI) with wastewater. Although phosphorus is considered a nutrient element important for the growth of humans, animals and plants, excessive phosphorus in lakes and other water bodies can lead to several environmental problems, such as eutrophication and the outbreak of cyanobacteria and red tide [2]. These problems can threaten drinking water safety and biodiversity in the water environment. Chromium(VI) is also a contaminant of concern in wastewater. Chromium(VI) has been proven to be extremely hazardous to human health, and it can cause ulcer formation, dermatitis, liver damage, bronchitis, and even cancer [3].

Considering the negative effects of phosphorus and chromium(VI), the Ministry of Environmental Protection of the People's Republic of China has stipulated that the concentrations of phosphorus and chromium(VI) in discharged wastewater must be below 0.1 and 0.5 $mg \cdot dm^{-3}$, respectively [4]. The National Health and Family Planning Commission of the People's Republic of China has stipulated that the concentration of chromium(VI) in drinking water be below 0.05 $mg \cdot dm^{-3}$ [5]. The improved removal of phosphorus and chromium(VI) from wastewaters could have significant benefits to the health of the population and water systems in China. Many advanced treatment technologies for phosphorus and chromium(VI) removal have been developed and applied. The main treatment technologies include biological treatment [6], chemical precipitation [7], membrane separation[8], ion exchange [9], and adsorption [10, 11].

Compared with the other technologies, adsorption is generally thought to offer a high removal efficiency at a low cost. The significant benefits of adsorption have been proven by several researchers. Most research in this field focuses on developing new adsorbents. Adsorbents that are suitable for a given application, have a high removal efficiency for the target contaminant, and are low cost could not only reduce the environmental threats of phosphorus and chromium(VI) but also expand the application areas of adsorption technology.

Fly ash is a solid waste generated from coal-fired power plants. Because the majority of energy in China comes from coal-fired power plants, in 2014, China produced approximately 58 million tons of fly ash, of which approximately 60% is reused in various applications. The storage of residual fly ash occupies large areas of cultivated land and contributes to local air and water pollution. Fly ash particles are spheroidal and have a large surface area. Besides, the main chemical components of fly ash are silicon oxide and aluminum oxide. Therefore, fly ash is also considered raw material for synthesizing low-cost adsorbents. Modifying fly ash into a suitable adsorbent can decrease the environmental pollution caused by fly ash, as well as reduce the cost of adsorption technology.

In this study, microspheroidal particles in fly ash were modified by a three-step process to make them a suitable adsorbent for both phosphorus and chromium(VI). Con-

sidering that these two contaminants often coexist in wastewater, the adsorption experiments used both single and competitive solute systems. The impact of parameters such as adsorption time, pH, and temperature on the adsorption performance was also examined in both single and competitive solute systems. Then, the adsorption kinetics and isotherm equations were used for the analysis of the adsorption process.

2. EXPERIMENTAL

Materials. Fly ash material was obtained from Taicang Harbor Golden Concord Electric Power Generation Co., Ltd. (Taicang, Jiangsu). The main chemical composition was as follows: SiO_2 (56.71 wt. %), Al_2O_3 (28.9 wt. %), CaO (2.34 wt. %), Fe_2O_3 (4.02 wt. %), Na_2O (0.46 wt. %), MgO (0.04 wt. %), K_2O (1.32 wt. %), and TiO_2 (1.07 wt. %). KH_2PO_4 (analytically pure) and $K_2Cr_2O_7$ (analytically pure) were dissolved in deionized water. The concentrations of phosphorus and chromium(VI) were both 20 $mg \cdot dm^{-3}$. The KOH and HDTMA (hexadecyl trimethyl ammonium bromide) solution was prepared by dissolving KOH (analytically pure) and HDTMA (analytically pure) in deionized water. The concentrations of KOH and HDTMA in solution were 5 $mol \cdot dm^{-3}$ and 0.066 $mol \cdot dm^{-3}$. The solutions for adjusting pH were obtained by dissolving (0.2 $mg \cdot dm^{-3}$) either NaOH (analytically pure) or HNO_3 (analytically pure) in deionized water.

Modifying of fly ash spheroidal particles. The fly ash spheroidal particles were modified by a three-step process as follows: First, to gain pure fly ash spheroidal particles, uncombusted carbon and other impurities in the original fly ash must be removed by mixing the fly ash with deionized water (water/fly ash weight ratio = 5) with stirring at 200 rpm at room temperature, after which the dispersion was left to stand. Afterward, the fly ash was removed by filtration through a 0.45-μm membrane and dried to constant weight at 105 °C. Then, the filtrate was purified, and we obtained pure fly ash spheroidal particles. Subsequently, they were mixed with a 5 $mol \cdot dm^{-3}$ KOH solution at 75 °C for 2 h (water/fly ash weight ratio = 10) with stirring at 200 rpm. In contrast to previous studies, the modified conditions control the alkaline reaction process and transmit the silicate alumina to the amorphous phase [12, 13]. Following this, the dispersion was also filtered through a 0.45-μm membrane. The solid reaction products were washed with large amounts of deionized water to remove residual alkali, and this washing was continued until pH of the wash water was approximately 7. Then, the solid was dried to constant weight at 105 °C to obtain alkali-modified fly ash spheroidal particles (hereinafter referred to as AFPs). Subsequently, approximately 60 g of AFPs were mixed with 250 cm^3 of HDTMA solution in a conical flask at 25 °C for 10 h with stirring at 200 rpm. Following this, the dispersion was filtered through a 0.45-μm membrane. The solid reaction products were washed with large amounts of deionized water. Then, the solid was dried to constant weight at room temperature to obtain the surface-modified fly ash spheroidal particles (hereinafter referred to as MFPs) [14, 15].

Material characterizations. The MFPs were characterized by X-ray diffraction (XRD), scanning electron microscopy-energy dispersive spectroscopy, and Fourier transform infrared (FT-IR) spectroscopy, as well as using a microiontophoresis apparatus and a particle size analyzer. The XRD patterns of the powder samples were acquired using a Shimadzu XD-3A diffractometer employing Cu-Kα radiation (λ = 1.54056 Å). The morphologies of the composites were observed with a JSM6480 scanning electron microscope, and FT-IR spectra were recorded on a Nicolet iS5 FT-IR spectrometer using pressed KBr discs. The surface zeta potentials were determined by a JS94H microiontophoresis apparatus (POWEREACH). The specific surface areas were measured using a particle size analyzer (Mastersizer).

Adsorption experiments. The adsorption experiments were conducted as typical batch trials in single and competitive solute systems. In single solute systems, the original concentrations of phosphorus and chromium(VI) solutions were both 20 mg·dm^{-3}, whereas, in competitive solute systems, the phosphorus and chromium(VI) coexist in one solution, and the concentrations were also 20 mg·dm^{-3}. In each adsorption trial, a quantity of the MFPs was dispersed in 10 cm^3 of a phosphorus and chromium(VI) solution in a 20 cm^3 Teflon bottle. The bottles were subsequently immersed in a water bath and agitated at 200 rpm. Following adsorption, each dispersion was filtered through a 0.45-μm membrane, and the phosphorus and chromium(VI) concentrations in the filtered solution were determined by ion chromatography using an ICS-2100 Thermo Fisher instrument. pH of the solutions ranged from 1 to 13. The adsorption temperature ranged from 30 to 60 °C, and the adsorption time from 0 to 240 min. The doses of MFP were 0.5–8 g·dm^{-3}.

3. EQUATIONS USED IN THE STUDY

The symbolic representation and equations used in this paper are list as below:

$$Q_t = \frac{(C_0 - C_t)V}{m} \tag{1}$$

$$Q_e = \frac{(C_0 - C_e)V}{m} \tag{2}$$

where, V, cm^3, is the solution volume, m, g, is the mass of the adsorbent, Q_t, mg·g^{-1}, is the mass of phosphorus or chromium(VI) adsorbed per unit mass of the adsorbent at time t, Q_e, mg·g^{-1}, is the mass of phosphorus or chromium(VI) adsorbed per unit mass of the adsorbent at equilibrium, C_0, mg·dm^{-3}, is the initial concentration of phosphorus or chromium(VI), C_t, mg·dm^{-3}, is the concentration of phosphorus or chromium(VI) at time t, C_e, mg·dm^{-3}, is the concentration of phosphorus or chromium(VI) at equilibrium.

The kinetics equations used in the study are as follows:

- The pseudo-first-order model [16]:

$$\ln(Q_{e\text{-exp}} - Q_t) = \ln(\mathrm{Q}_{e\text{-cal}}) - k_1 t \tag{3}$$

where k_1, min^{-1}, is the rate constant of the first-order model.

- The pseudo-second-order model [17]:

$$\frac{t}{Q_t} = \frac{1}{k_2 Q_{e\text{-cal}}^2} + \frac{t}{Q_{e\text{-cal}}} \tag{4}$$

where k_2, $\mathrm{g \cdot mg^{-1} \cdot min^{-1}}$, is the rate constant of the second-order model.

The optimal kinetics model could be chosen based on the regression coefficient (R^2) and root mean square error (RMSE) [18, 19]. The R^2 was determined with fitting software, and the value that is more close to 1 corresponds to the model that is more suitable for explaining the adsorption process. The RMSE is defined as follows:

$$\mathrm{RMSE} = \left(\frac{\sum_{1}^{N} (Q_{e\text{-exp}} - Q_{e\text{-cal}})^2}{N} \right)^{1/2} \tag{5}$$

Lower RMSE values indicate that the results obtained from a model are closer to the actual experimental data.

The adsorption isotherm equations are as follows:

- Langmuir isotherm

$$Q_e = \frac{k_L Q_m C_e}{1 + k_L C_e} \tag{6}$$

where Q_e, $\mathrm{mg \cdot g^{-1}}$, is the mass of phosphorus or chromium(VI) adsorbed per unit mass of the adsorbent at adsorption equilibrium; C_e, $\mathrm{mg \cdot dm^{-3}}$, is the concentration of phosphorus or chromium(VI) at adsorption equilibrium, Q_m, $\mathrm{mg \cdot g^{-1}}$, is the maximum adsorption capacity. k_L, $\mathrm{dm^3 \cdot mg^{-1}}$, is the Langmuir constant related to the energy of adsorption.

After modification, we arrive at

$$\frac{C_e}{Q_e} = \frac{1}{k_L Q_m} + \frac{C_e}{Q_m} \tag{7}$$

The equation of the Freundlich isotherm is as follows:

$$Q_e = k_F C_e^{1/n} \tag{8}$$

where k_F, mg·g^{-1}·mg·dm^{-3} and n are constants indicative of the adsorption capacity and adsorption intensity.

After modifications we obtain

$$\ln Q_e = \ln k_F + \frac{1}{n} \ln C_e \tag{9}$$

The equations of competitive Langmuir isotherms [20, 21] are as follows:

$$Q_{e\text{-Cr}} = \frac{k_{L\text{-Cr}} Q_{m\text{-Cr}} C_{e\text{-Cr}}}{1 + k_{L\text{-Cr}} C_{e\text{-Cr}} + k_{L\text{-P}} C_{e\text{-P}}} \tag{10}$$

$$Q_{e\text{-}P} = \frac{k_{L\text{-P}} Q_{m\text{-P}} C_{e\text{-P}}}{1 + k_{L\text{-P}} C_{e\text{-P}} + k_{L\text{-Cr}} C_{e\text{-Cr}}} \tag{11}$$

where $Q_{e\text{-}i}$, mg·g^{-1}, is the mass of element i adsorbed per unit mass of the adsorbent at adsorption equilibrium in a competitive adsorption system, $C_{e\text{-}i}$, mg·dm^{-3}, is the concentration of element i at adsorption equilibrium in a competitive adsorption system, $Q_{m\text{-}i}$, mg·g^{-1}, is the maximum adsorption capacity of element i in a competitive adsorption system, $k_{L\text{-}i}$, dm^3·mg^{-1}, is the competitive Langmuir constant related to the element i.

After some modifications of equation (11), we obtain:

$$\frac{C_{e\text{-Cr}}}{Q_{e\text{-Cr}}} = \frac{1}{k_{L\text{-Cr}} Q_{m\text{-Cr}}} + \frac{C_{e\text{-Cr}}}{Q_{m\text{-Cr}}} + \frac{k_{L\text{-P}} C_{e\text{-P}}}{k_{L\text{-Cr}} Q_{m\text{-Cr}}} \tag{12}$$

$$\frac{C_{e\text{-P}}}{Q_{e\text{-P}}} = \frac{1}{k_{L\text{-P}} Q_{m\text{-P}}} + \frac{C_{e\text{-P}}}{Q_{m\text{-P}}} + \frac{k_{L\text{-Cr}} C_{e\text{-Cr}}}{k_{L\text{-P}} Q_{m\text{-P}}} \tag{13}$$

4. RESULTS AND DISCUSSION

4.1. CHARACTERIZATION OF MFP

Figure 1 shows the SEM images of the original fly ash, an AFP, and an MFP. In Figs. 1a, b, spheroidal particles with a relatively smooth surface are observed. After the alkali modification process, abundant amorphous gels are found in Fig. 1c, and the sur-

face of the residual spheroidal particles is also wrapped with the amorphous gels. According to the previous study and reference, the amorphous gels should be the silicate alumina "precursors" of a crystalline zeolite [12]. The modified conditions (water/fly ash = 10) control the alkaline reaction process and transmit the silicate alumina to the amorphous phase [13]. Meanwhile, because the microshapes change from spheroidal to rectangular ones, the microsurface area of AFPs grows from the original 3 to 380 $m^2 \cdot kg^{-1}$ (obtained from a particle size analyzer). Comparing Figs. 1c and 1d, no clear differences are observed between the AFP and MFP. The MFP keeps the surface morphology after the HDTMA modification process.

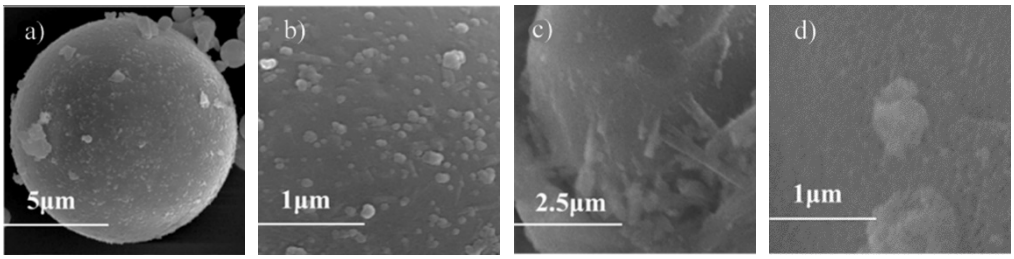

Fig. 1. SEM morphologies of the original fly ash (a, b), AFP (c) and MFP (d)

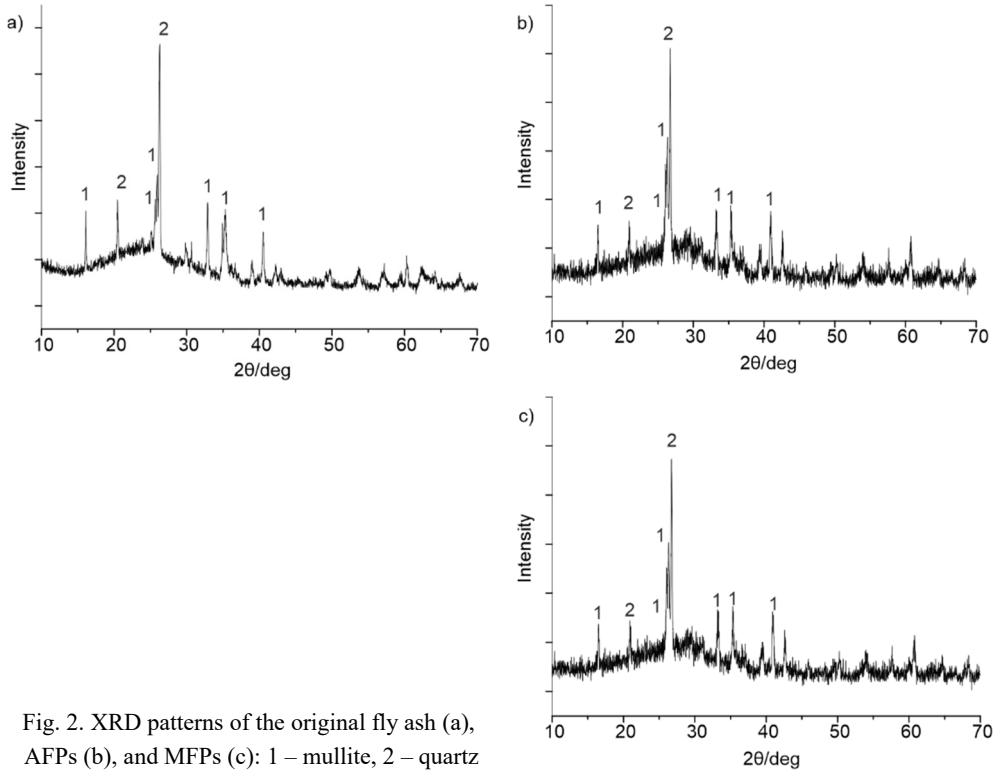

Fig. 2. XRD patterns of the original fly ash (a), AFPs (b), and MFPs (c): 1 – mullite, 2 – quartz

Figure 2 shows the XRD patterns of the original fly ash, AFPs, and MFPs. Crystalline phases observed in all three samples are indexed for quartz and mullite using the standard JCPDS (Card Nos. 65-0466 and 15-0776). Characteristic peaks are related to 2θ at approximately (26.603°), (20.822°), and (50.103°) for quartz and to 2θ at approximately (26.181°), (25.940°), and (40.801°) for mullite. The results indicate that there is no crystalline phase change during the surface modification process. Otherwise, the glass phase in the original fly ash shows no diffraction peaks but a broad "halo" at 2θ approximately 20–40°. The decreasing strength of the broad "halo" in the AFP patterns implies the dissolving of the glass phase during the alkali modification process. Furthermore, no new crystalline phase is found, suggesting that under the limit of the modified conditions (mass water/fly ash = 10), the reaction products of the alkali modification process should be an amorphous phase (as seen in Fig. 1c), which is insensitive to XRD technology.

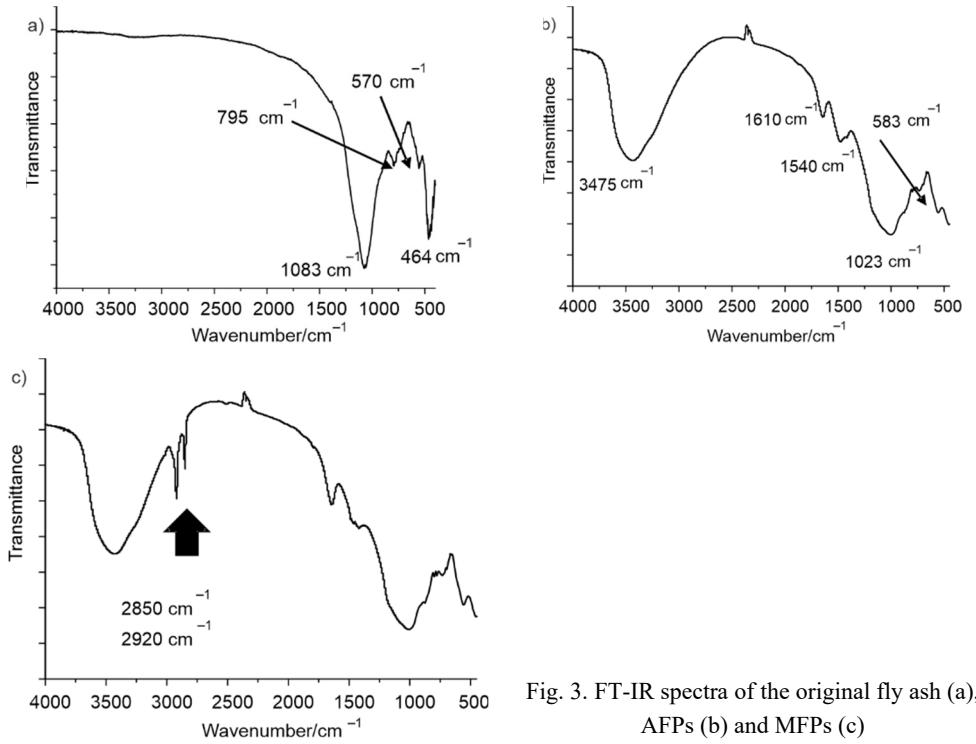

Fig. 3. FT-IR spectra of the original fly ash (a), AFPs (b) and MFPs (c)

Figure 3 presents the FT-IR spectra of the original fly ash, AFPs, and MFPs. Intense peaks observed in the spectrum of the original fly ash are at 1083, 795, 570, and 464 cm^{-1}. The peak at 1083 cm^{-1} should be attributed to the T–O (where T is Si or Al) stretching mode. The double peak at 795 cm^{-1} should be attributed to quartz. The peak at 570 cm^{-1} should be attributed to mullite, and the peak at 464 cm^{-1} should be attributed to a SiO_4 tetrahedron

(O–Si–O) deformation mode [22]. After the alkali modification process, the FT-IR spectrum of AFPs shows peaks at 3475, 1610, 1540, 1023, and 583 cm^{-1}. The broad peak at 3475 cm^{-1} and others at 1610 and 1540 cm^{-1} correspond to the stretching vibration and bending vibrations of O–H [23]. The peaks assigned to the Si(Al)–O–Si(Al) stretching vibration and the O–Si(Al)–O bending mode can be observed at 1023 and 583 cm^{-1} [24]. These peaks correspond to amorphous silica alumina gel forming during the alkali modification process. The evident differences between the FT-IR spectra of AFPs and MFPs can be found at 2850 and 2920 cm^{-1}. The sharp peaks at 2850 and 2920 cm^{-1} are assigned to the $–CH_2–$ group in HDTMA [25], which implies that the HDTMA was deposited on the surface of the fly ash spheroidal particles.

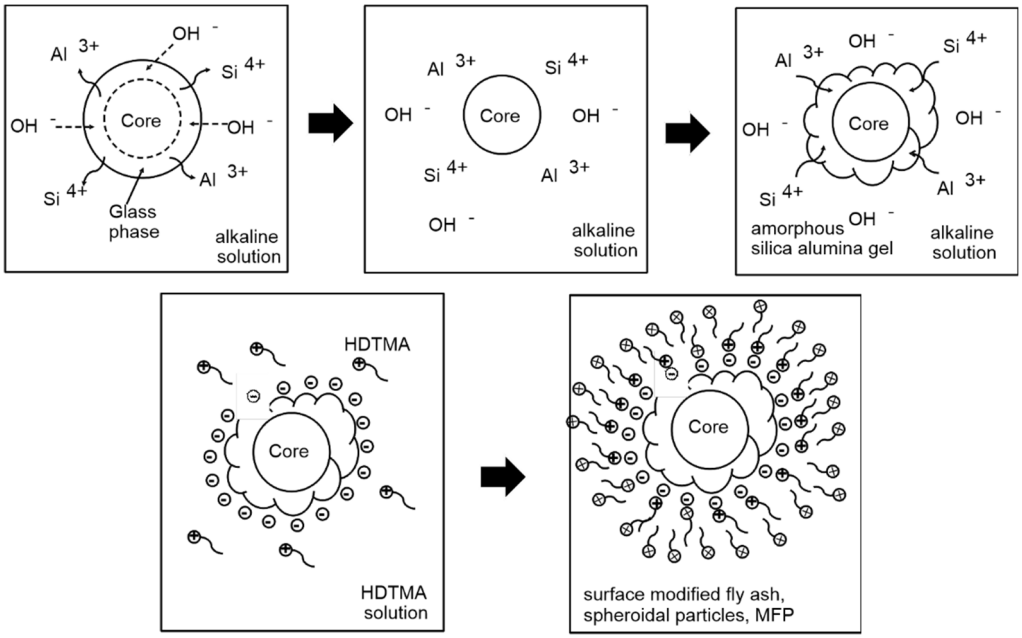

Fig. 4. Modification processes of fly ash spheroidal particles:
top: alkali-modified process, bottom: HDTMA-modified process

Based on the above analysis, the modification process of fly ash spheroidal particles can be concluded as shown in Fig. 4. At the initial stage, the fly ash particles react with the alkaline solution, which leads to the dissolving of Si^{4+} and Al^{3+} from the glass phase of fly ash particles to the solution environment. Subsequently, with their concentrations continuously increasing, Si^{4+} and Al^{3+} ions in the solution environment tend to form an amorphous silica alumina gel and deposit on the surface of residual fly ash spheroidal particles (as AFPs). Due to the potential equilibrium, the surface of AFPs shows a negative charge in the solution. Such a negatively charged surface can only adsorb pollutants with a positive charge, such as heavy metal ions, and is almost invalid to pollutants

with a negative charge, such as phosphorus and chromium(VI) ions. To optimize the surface charge, the AFPs must be modified by the HDTMA solution. With the HDTMA adsorbed on the AFPs, the negative charge of the surface is balanced with the positively charged head group of HDTMA. As a consequence of additional HDTMA precipitation, HDTMA bilayers or patchy bilayers form on the surface of AFPs, and then, the positively charged head groups of later precipitated HDTMA transform the surface charge of AFPs from negatively charged to positively charged (MFPs) [14]. As Figure 5 shows, before modification by HDTMA, the surface zeta potential of AFPs appears as a miniscule positive charge (when the solution pH is lower than approximately 5.5) and a strong negative charge (when the solution pH is higher than approximately 5.5). This surface charge could lead to the adsorption tendency of molecules (H_2CrO_4 and H_3PO_4) and anions ($HCrO_4^-$, CrO_4^{2-}, $Cr_2O_7^{2-}$, $H_2PO_4^-$, HPO_4^{2-}, and PO_4^{3-}) on AFPs to become very difficult. In contrast, after modification by HDTMA, the surface zeta potential of MFPs is drastically positively charged except for a minutely negatively charged surface still found in a solution environment at high pH. Considering the electrostatic attraction effect, the excellent anion adsorption ability of MFPs can be believed and will be proven by the experimental results below.

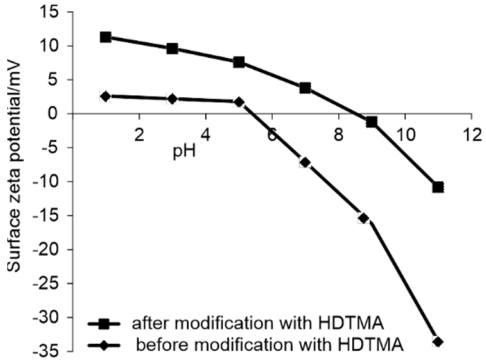

Fig. 5. Surface zeta potentials of AFPs (before being modified by HDTMA) and MFPs (after being modified by HDTMA)

4.2. pH OF THE SOLUTIONS

pH of the solution is recognized to be an important factor affecting the adsorption efficiency of phosphorus anions and chromium(VI) anions on MFPs. In our study, the role of solution pH (1–13) is examined in both single and competitive solute systems. The adsorption temperature and MFP concentration are 50 °C and 4 g·dm^{-3}. As clearly seen from Fig. 6, in single chromium(VI) anion systems, the adsorption efficiency continuously decreases with the pH increasing from 1 to 13. The adsorption efficiency at pH = 1 is approximately 98%, which is higher than 87% at pH = 5 and 66% at pH = 13. Similar results can be observed in single phosphorus anion systems. The adsorption efficiencies of phosphorus anions at pH = 1, 5, and 13 are approximately 93%, 74%, and 6.6%, respectively.

The factors influencing the adsorption efficiency for solute anions and solid adsorbent can be concluded as follows: the surface property of the adsorbent, the solute species of anions and the other competitive solute anions. First, the surface charge of the adsorbent has long been known to be an important factor influencing the adsorption efficiency. Regularly, the surface charge of the adsorbent can be examined by the zeta potential. From Fig. 5, it can be seen that with the solution pH increasing from 1 to 13, the surface zeta potential of MFPs shows a decreasing tendency. The pH_{zpc} of MFPs can be found when the solution pH is approximately 8.5. This means that the surface of the MFPs should be positively charged when the solution pH is lower than 8.5, while negatively charged surface can be observed when the solution pH is higher than 8.5. Theoretically, the positively charged adsorbent surface can extremely force the formation of complexes between anions and chemical groups loaded on the adsorbent surface, and many complexes would result in excellent adsorption efficiency. This interaction means that a higher positive zeta potential would greatly attract the anions, while the adsorption process would be impeded by a negatively charged surface. Therefore, the adsorption efficiency of chromium(VI) anions and phosphorus anions can be understood to continuously decrease with the solution pH ranging from 1 to 13, and this notion is consistent with the experimental results.

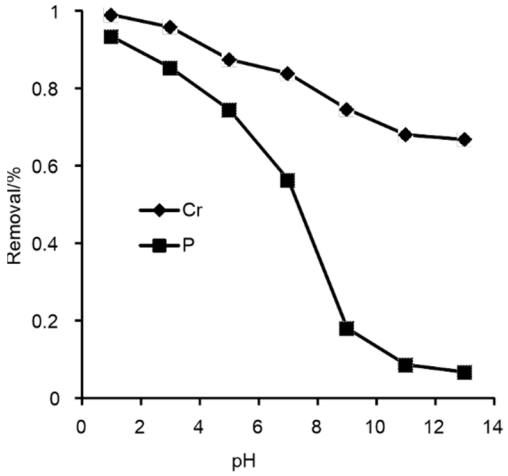

Fig. 6. Effects of pH on the adsorption of phosphorus and chromium(VI) on MFP (single solute systems)

Second, in aqueous solution, the forms of phosphorus and chromium(VI) anions are extremely related to pH. For the phosphorus solutions, the following equilibria occur [26]:

$$H_3PO_4 \xleftrightarrow{K_1} H_2PO_4^- + H^+ \tag{14}$$

$$H_2PO_4^- \xleftrightarrow{K_2} HPO_4^{2-} + H^+ \tag{15}$$

$$HPO_4^{2-} \xleftrightarrow{K_3} PO_4^{3-} + H^+ \quad (16)$$

where pK_1 = 2.12, pK_2 = 7.21, and pK_3 =12.3.

Because of these ionic equilibria, the dominant species in the phosphorus solution change as the pH increases. When the pH < 3, the dominant species is H_3PO_4. Then, $H_2PO_4^-$ becomes the dominant species when pH ranges from 3 to 7. With the pH increasing above 8, the dominant species changes to HPO_4^{2-}. Finally, the PO_4^{3-} replaces the HPO_4^{2-} after the solution pH reaches higher than 12. Similarly, in the chromium(VI) solution, the present species include H_2CrO_4 $HCrO_4^-$, CrO_4^{2-} and $Cr_2O_7^{2-}$, and the dominant species also vary strictly depending on the following chemical equilibrium functions [27].

$$H_2CrO_4 \xleftrightarrow{K_4} HCrO_4^- + H^+ \quad (17)$$

$$HCrO_4^- \xleftrightarrow{K_5} CrO_4^{2-} + H^+ \quad (18)$$

$$Cr_2O_7^{2-} + H_2O \xleftrightarrow{K_6} 2HCrO_4^- \quad (19)$$

where pK_4 = 4.1, pK_5 = 5.9, and pK_6 = 2.2.

Based on the ionic equilibrium calculations and references, CrO_4^{2-} has been proved to be the major ions when then solution pH is higher than 6. $HCrO_4^-$ become the major ions when pH is between 2 and 6. Trace H_2CrO_4 species can be found at pH < 2. Additionally, a small amount of $Cr_2O_7^{2-}$ ions coexists with $HCrO_4^-$ and CrO_4^{2-} ions when pH is lower than approximately 7. According to the analysis above, the ionic charge of phosphorus and chromium(VI) anions decreases as pH increases (the sequence is as follows: H_3PO_4 to $H_2PO_4^-$ to HPO_4^{2-} to PO_4^{3-} and H_2CrO_4 to $HCrO_4^-$ to CrO_4^{2-}).

Generally, in a typical solid–liquid phase adsorption system, the anions with the higher negative charge are more likely to be adsorbed by the adsorbent with the positive charge on the surface. Thus, the adsorption efficiency of PO_4^{3-} and CrO_4^{2-} is higher than that of the other anions. However, there are still some differences between the theoretical analysis and practical experimental results. The reason why there are differences is that the adsorption efficiency of anions in the solution is affected by not only the charge of anions but also the surface properties of the adsorbent, the existence of competitive ions, and some other factors. Though the anions PO_4^{3-} and CrO_4^{2-} certainly present higher negative charges than other anions, PO_4^{3-} and CrO_4^{2-} both exist in the solution with a pretty high value of pH. The potential of the MFP surface shows an evident negative-charge property (Fig. 5). A surface with negative charges will hinder the adsorption process of anions because of electrostatic repulsion, which leads to a decrease in the adsorption efficiency. These results imply that the adsorption ability of MFPs towards

anions at higher pH is extremely less than that at lower pH. This phenomenon should be related to the surface property of MFPs.

Apart from the solute species and surface charge, competitive ions should also be recognized as an important factor affecting the adsorption efficiency. The competitive ions generally fall into two categories: the original anions existing in solution and the anions added into the solution. OH^- is the most common original competitive anion present during the adsorption process. Because of its small ionic radius, OH^- is adsorbed by the adsorbent significantly more readily than the other anions, and then, extremely influences the adsorption efficiency of anions.

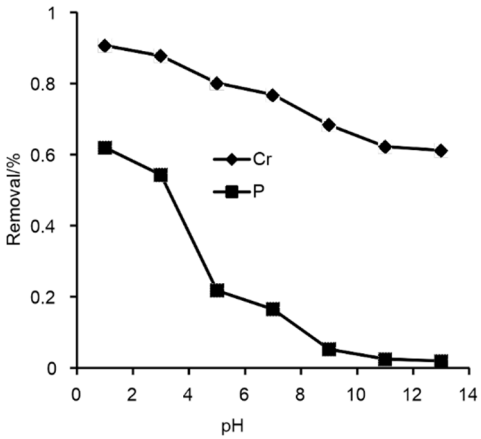

Fig. 7. Effects of pH on the adsorption of phosphorus and chromium(VI) on MFPs (competitive solute systems)

Similar to the original anions, the anions added into the solution can also affect the adsorption process. Figure 7 shows the effects of pH on the adsorption of phosphorus and chromium(VI) anions by MFPs in competitive solute systems (coexisting phosphorus and chromium(VI)). The adsorption efficiency still presents a decreasing tendency as the solution pH increases from 1 to 13. This appearance can still be attributed to the increasing concentration of OH^-. The adsorption efficiencies of competitive solute systems are substantially lower than those of single solute systems. For chromium(VI), when pH is 3 and 9, the values of the adsorption efficiency in a competitive solute system are approximately 87.8% and 68.4%, while in single solute systems, – 97.8% and 74.6%. A similar result can be obtained from the phosphorus adsorption process. In single solute systems, the adsorption efficiency can reach 85.3% and 56.5% when the pHs are 3 and 7; however, in a competitive solute system, the adsorption efficiency can only reach 54.3% and 16.5%. An even more important item is that in a single solute system, the maximum adsorption efficiency of phosphorus anions can achieve approximately 93.4%; however, in a competitive solute system, the adsorption efficiency limit is 62%. These results imply that the adsorption process of phosphorus is extremely influenced by chromium(VI) anions, and a satisfactory adsorption efficiency is very difficult to achieve.

4.3. TEMPERATURE AND ADSORPTION KINETICS

Figures 8 and 9 show the effect of the temperature on the adsorption efficiency. An increase in temperature and adsorption time can improve the adsorption efficiency, no matter whether in single or competitive solute systems.

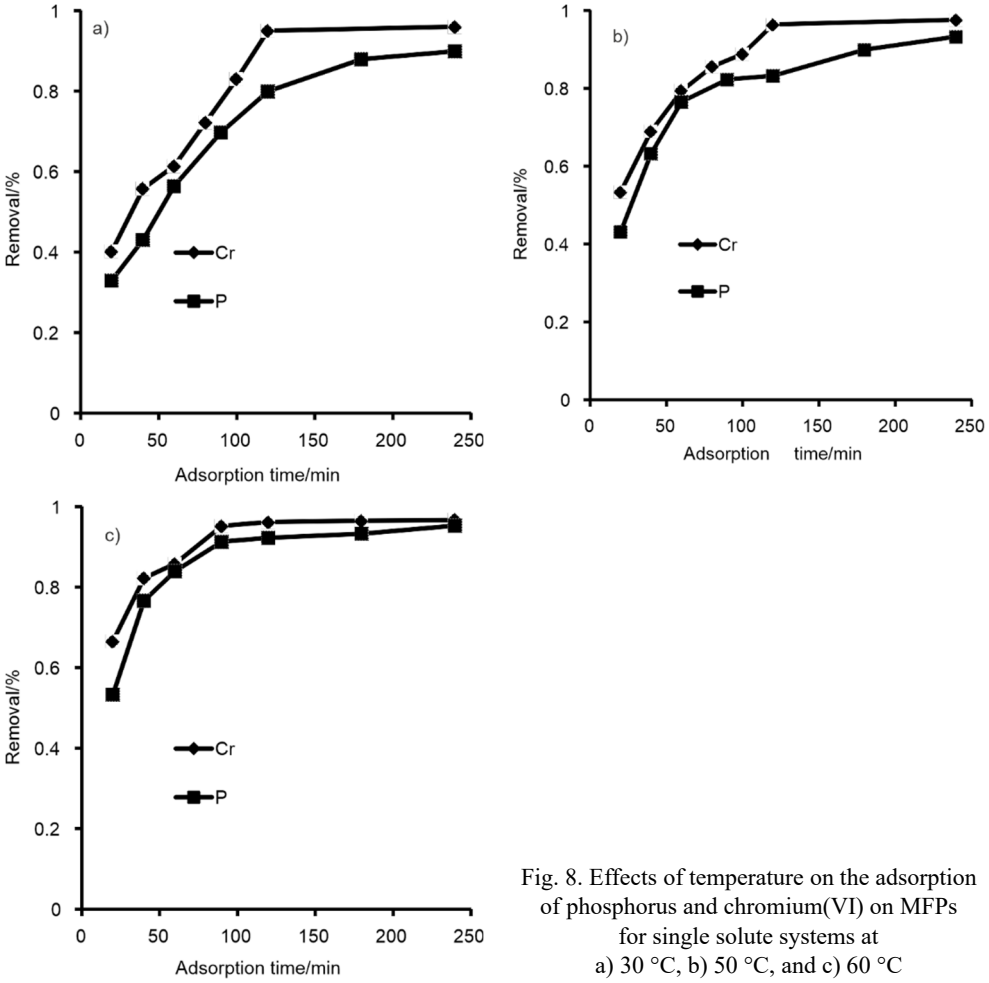

Fig. 8. Effects of temperature on the adsorption of phosphorus and chromium(VI) on MFPs for single solute systems at a) 30 °C, b) 50 °C, and c) 60 °C

For example, in the chromium(VI) single system, the adsorption efficiency is approximately 61.6% after 60 min at 30 °C. Then, the adsorption efficiency improves to approximately 85.8% or 96% when the temperature increases to 60 °C or the adsorption time increases to 240 min. Similarly, in the phosphorus single system, after the temperature increases from 30 to 60 °C, the adsorption efficiencies at 40 min and 90 min are improved from 43.1% and 69.8% to 76.6% and 91.3%. When the adsorption time is

increased from 60 min to 240 min, the adsorption efficiency of phosphorus increases from 43% to 89.9% at 30 °C and from 63.2% to 93.2% at 50 °C. Comparing the chromium(VI) and phosphorus single systems, it can be found that the chromium(VI) maintains a slightly higher adsorption efficiency than the phosphorus does during the whole adsorption process. The results imply that the affinity of chromium(VI) to the adsorption active sites on MFPs is stronger than that of phosphorus. The adsorption efficiency difference between chromium(VI) and phosphorus distinctly appears in competitive solute systems.

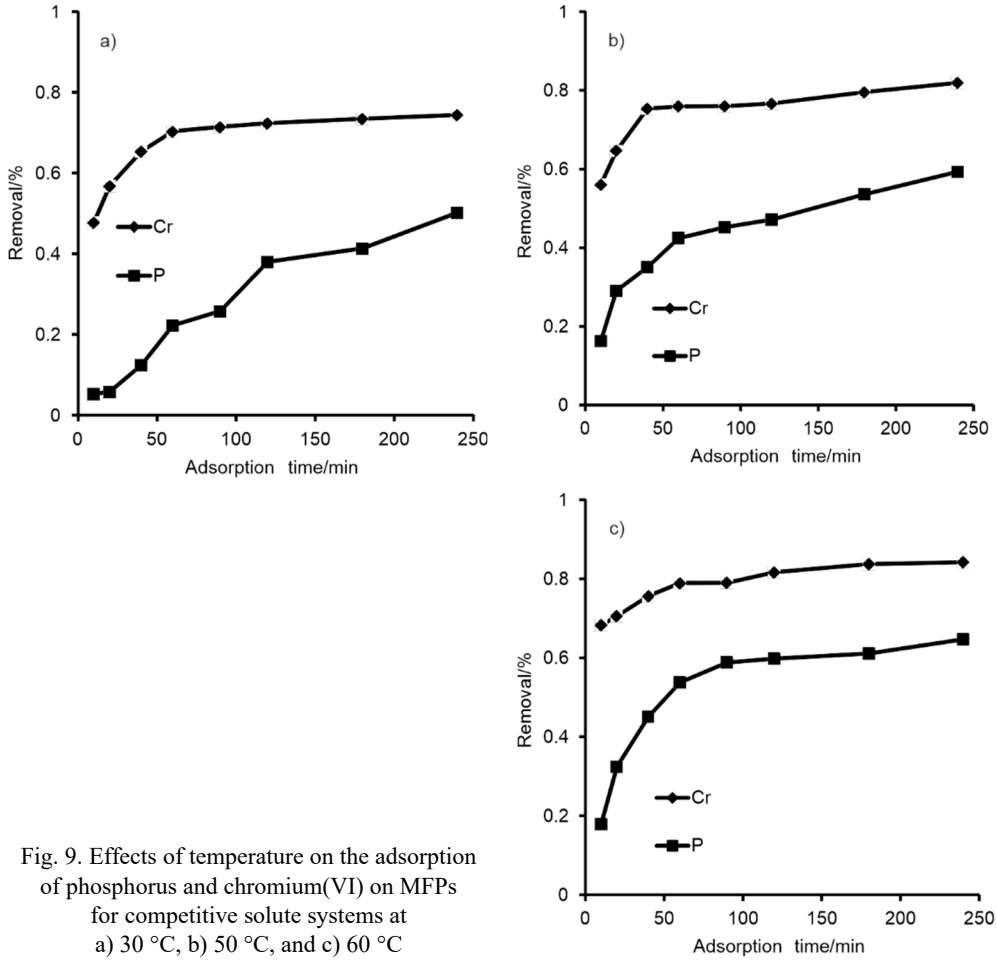

Fig. 9. Effects of temperature on the adsorption of phosphorus and chromium(VI) on MFPs for competitive solute systems at a) 30 °C, b) 50 °C, and c) 60 °C

From Figure 9, it can be seen that in the competitive solute systems, the adsorption efficiency of chromium(VI) maintains a relatively high level, while the adsorption efficiency of phosphorus decreases substantially. For example, at 50 °C, the adsorption efficiencies of chromium(VI) remain at approximately 75.9% and 81.9% after 60 min and 240 min. In contrast, the adsorption efficiencies of phosphorus are only approximately

42.4% and 59.3% under similar conditions. A similar phenomenon can be observed under every condition, which provides further evidence that adsorption of phosphorus is more difficult than that of chromium(VI). Chromium(VI) can form a stronger complex with the adsorption active sites on MFPs. On the other hand, according to a comparison of Figs. 8 and 9, we can discover that the adsorption efficiencies of phosphorus and chromium(VI) on MFPs can reach more than 95% and even close to 100% by improving the adsorption temperature and lengthening the adsorption time for a single adsorption system. However, in a competitive solute system, though the improvement in adsorption temperature and the lengthening of the adsorption time still can increase the adsorption efficiency, and the final saturated adsorption efficiency of 90% is difficult to surpass. As is seen from Fig. 9, at 60 °C, the highest adsorption efficiencies of phosphorus and chromium(VI) can only reach 64.1% and 84.4%, respectively, and the increasing trend of adsorption efficiency becomes very weak after 180 min.

Table 1

Adsorption kinetic parameters calculated based on the pseudo-first-order and pseudo-second-order models

Single solute systems										
Ion	T [°C]	$Q_{e\text{-exp}}$ [mg·g^{-1}]	Pseudo-first-order				Pseudo-second-order			
			k_1 [min^{-1}]	$Q_{e\text{-cal}}$ [mg·g^{-1}]	R^2	RMSE	k_2 [g·mg^{-1}·min^{-1}]	$Q_{e\text{-cal}}$ [mg·g^{-1}]	R^2	RMSE
Cr	30	5	0.0133	3.36	0.8157	1.64	0.00434	5.7	0.9854	0.7
	50	5	0.0138	2.26	0.8546	2.74	0.00964	5.32	0.9981	0.32
	60	5	0.0102	1.161	0.7384	3.039	0.0149	5.05	0.9993	0.05
P	30	5	0.0092	3.7	0.9597	1.3	0.00322	5.62	0.9936	0.62
	50	5	0.0089	2.49	0.9311	2.51	0.00788	5.133	0.9988	0.133
	60	5	0.0091	1.598	0.8047	3.402	0.0228	5.05	0.9988	0.05
Competitive solute systems										
Ion	T [°C]	$Q_{e\text{-exp}}$ [mg·g^{-1}]	Pseudo-first-order				Pseudo-second-order			
			k_1 [min^{-1}]	$Q_{e\text{-cal}}$ [mg·g^{-1}]	R^2	RMSE	k_2 [g·mg^{-1}·min^{-1}]	$Q_{e\text{-cal}}$] [mg·g^{-1}]	R^2	RMSE
Cr	30	4.5	0.0036	1.562	0.6769	2.938	0.0424	3.81	0.9999	0.69
	50	4.5	0.005	2.35	0.7675	2.15	0.0401	4.14	0.9992	0.36
	60	4.5	0.0057	0.952	0.9049	3.548	0.0492	4.28	0.9975	0.22
P	30	3.5	0.0052	3.417	0.9773	0.083	0.00072	5.31	0.7229	1.81
	50	3.5	0.0062	1.212	0.9577	2.288	0.00935	3.24	0.9914	0.26
	60	3.5	0.0089	0.991	0.8603	2.509	0.01207	3.54	0.9997	0.04

In our study, pseudo-first-order and pseudo-second-order kinetic models have been applied to fit the experimental data. As seen in Table 1, in single and competitive solute systems, the pseudo-second-order model shows better fitting results than does the pseudo-first-order model at every temperature. The R^2 values of the pseudo-second-order model are all higher than 0.98 (except for the phosphorus adsorption process at

lower than 30 °C in competitive solute systems), while all the R^2 values of the pseudo--first-order model are relatively lower. Moreover, the RMSE of the pseudo-second-order model is lower than that of the pseudo-first-order model, which means that the calculated saturated adsorption capacity gained from the pseudo-second-order model is significantly closer to the practical value and that the pseudo-second-order model can better describe the adsorption processes of phosphorus and chromium(VI) on MFPs.

4.4. ADSORPTION ISOTHERMS

Figures 10 and 11 show adsorption isotherms of chromium(VI) and phosphorus on MFPs in single solute systems. The Langmuir adsorption isotherm equation can better simulate the adsorption processes of phosphorus and chromium(VI) on MFPs.

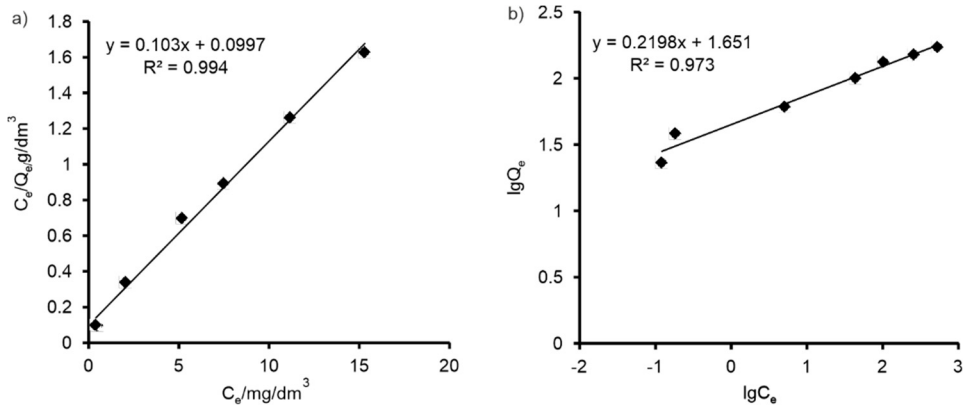

Fig. 10. Adsorption isotherms of chromium(VI):
a) Langmuir isotherm model, b) Freundlich isotherm model

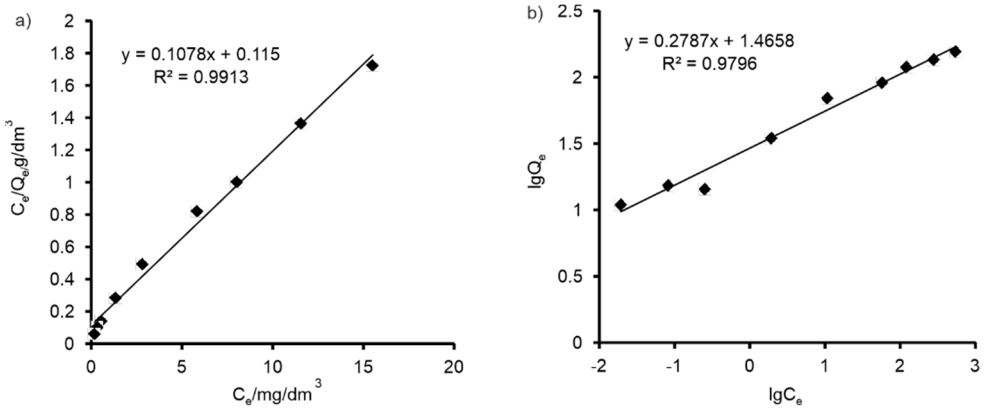

Fig. 11. Adsorption isotherms of phosphorus:
a) Langmuir isotherm model, b) Freundlich isotherm model

The values of R^2 (Langmuir) are 0.9913 and 0.994 for phosphorus and chromium(VI), which are higher than those for the Freundlich isotherms. The maximum adsorption capacities (Q_m) of chromium(VI) and phosphorus are 9.71 mg·g^{-1} and 9.28 mg·g^{-1}, respectively. The adsorption ability of chromium(VI) on MFPs is a little stronger than that of phosphorus. Finally, the results are consistent with the previous experimental data. Because chromium(VI) and phosphorus can better obey the Langmuir adsorption isotherm in single solute systems, the competitive Langmuir isotherm equation is applied to fit the adsorption process of chromium(VI) and phosphorus in a competitive solute system. The adsorption capacity of chromium(VI) ($Q_{e\text{-Cr}}$) on MFPs is no longer a unitary function of the equilibrium concentration ($C_{e\text{-Cr}}$) but transforms into binary functions that are concerned with the equilibrium concentration of chromium(VI) ($C_{e\text{-Cr}}$) and phosphorus ($C_{e\text{-P}}$). The binary function analysis results are shown in Fig. 12.

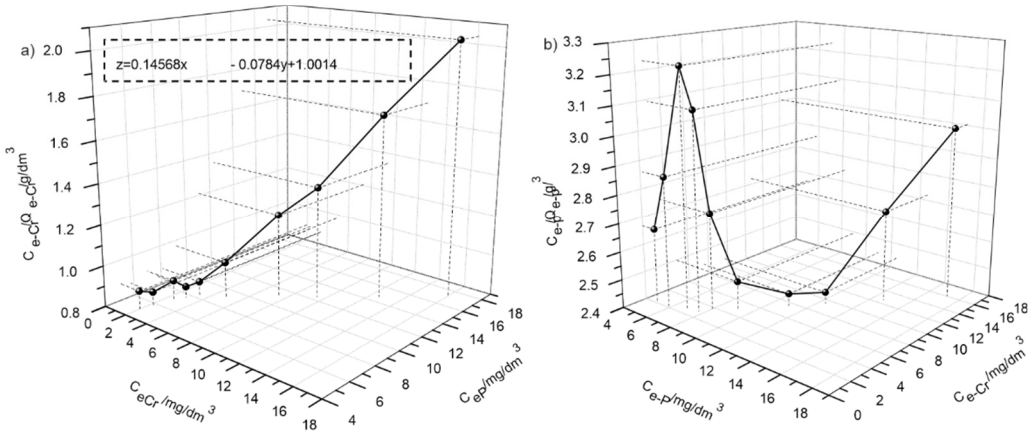

Fig. 12. Results of the adsorption analysis for the competitive Langmuir isotherm model: a) chromium(VI), b) phosphorus

In a competitive solute system, the maximum adsorption capacity of chromium(VI) on MFPs decreases from 9.70 mg·g^{-1} to 6.86 mg·g^{-1}. Chromium(VI) cannot monopolize all the active adsorption sites and must compete with phosphorus. On the other hand, in a competitive adsorption system, there is no accepted result that can be achieved for phosphorus, and the result appears as divergent data (Fig. 12b). Consequently, in a competitive solute system, because of the disturbing effect of chromium(VI), the adsorption process of phosphorus on MFPs no longer strictly fits the Langmuir adsorption isotherm equations.

5. CONCLUSION

The surface of fly ash spheroidal particles is modified by surface structural reconstitution and zeta potential optimization. After the surface structural reconstitution, the

surfaces of spheroidal particles (AFPs) are wrapped with amorphous gels, and the microsurface area of the particles increases from 3 $m^2 \cdot kg^{-1}$ to 380 $m^2 \cdot kg^{-1}$. Via reacting with the HDTMA solution, the positively charged head groups of precipitated HDTMA can transform the surface charge of the spheroidal particles (MFPs) from negatively charged to positively charged, which can adsorb electronegative anions from the solution. No matter whether a single or competitive solute system, the adsorption efficiency continuously decreases as pH increases. The surface zeta potential and existence of competitive ions should be recognized as two important factors affecting the adsorption efficiency. Chromium(VI) was more easily adsorbed by MFPs. The adsorption efficiencies of chromium(VI) and phosphorus in single and competitive solute systems can be improved by increasing temperature; however, compared with a single solute system, the final equilibrium adsorption efficiency of a competitive solute system reaches more than 90% only with difficulty. Based on the whole adsorption process (single and competitive systems), the fitting results of the pseudo-second-order model show better agreement than does the pseudo-first-order model at every temperature. The adsorption process of phosphorus and chromium(VI) on MFPs in single adsorption systems can be better simulated by the Langmuir adsorption isotherm; however, in competitive solute systems, the competitive Langmuir adsorption isotherm can only could be applied to the chromium(VI) adsorption process.

ACKNOWLEDGMENT

This work was financially supported by the Natural Science Foundation of China (Grant No. 21407068), 2016 University of Jiangsu Province Blue Project of young academic leader training objects, Jiangsu Science and Technology Program – a prospective joint research project (Grant No. BY2016068-01), Open Fund Project of Jiangsu Provincial Key Laboratory of Environmental Engineering (Grant No. KF2014002, KF2015011), 13th Five-Year Plan key project of Jiangsu City Vocational College (Grant No. 16SSW-Z-001).

REFERENCES

[1] Environmental Protection Ministry of China, *National Environmental Statistics Bulletin*, 2014.

[2] MULLAN A., MCGRATH J.W., ADAMSON T., IRWIN S., QUINN J.P., *Pilot-scale evaluation of the application of low pH-inducible polyphosphate accumulation to the biological removal of phosphate from wastewaters*, Environ. Sci. Technol., 2006, 40 (1), 296–301.

[3] KHEZAMI L., CAPART R., *Removal of chromium(VI) from aqueous solution by activated carbons: kinetic and equilibrium studies*, J. Hazard. Mater., 2005, 123 (1–3), 223–231.

[4] Ministry of Environmental Protection of the People's Republic of China, *Integrated wastewater discharge standard (GB 8978-1996)*, 1996.

[5] National Health and Family Planning Commission of the People's Republic of China, *Standards for drinking water quality (GB5749-2006)*, 2007.

[6] LANHAM A.B., OEHMEN A., SAUNDERS A.M., CARVALHO G., NIELSEN P.H., *Metabolic versatility in full-scale wastewater treatment plants performing enhanced biological phosphorus removal*, Water Res., 2013, 47 (19), 7032–7041.

[7] YE Z.L., CHEN S.H., WANG S.M., LIN L.F., YAN Y.J., *Phosphorus recovery from synthetic swine wastewater by chemical precipitation using response surface methodology*, J. Hazard. Mater., 2010, 176 (1–3), 1083–1088.
[8] GHERASIM C.V., BOURCEANU G., OLARIU R.I., ARSENE C., *A novel polymer inclusion membrane applied in chromium(VI) separation from aqueous solutions*, J. Hazard. Mater., 2011, 197 (6), 244–253.
[9] KORAK J.A., HUGGINS R., ARIAS-PAIC M., *Regeneration of pilot-scale ion exchange columns for hexavalent chromium removal*, Water Res., 2017, 118, 141–151.
[10] REN G., WANG X., HUANG P., ZHONG B., ZHANG Z., *Chromium(VI) adsorption from wastewater using porous magnetite nanoparticles prepared from titanium residue by a novel solid-phase reduction method*, Sci. Total Envir., 2017, S607–608, 900–910.
[11] FANG H., CUI Z., HE G., HUANG L., CHEN M., *Phosphorus adsorption onto clay minerals and iron oxide with consideration of heterogeneous particle morphology*, Sci. Total Envir., 2017, S605–606, 357–367.
[12] CHEN C., GONG W., LUTZE W., PEGG I.L., *Kinetics of fly ash geopolymerization*, J. Mater. Sci., 2011, 46 (9), 3073–3083.
[13] CHEN C., GONG W., LUTZE W., PEGG I.L., ZHAI J., *Kinetics of fly ash leaching in strongly alkaline solutions*, J. Mater. Sci., 2010, 46 (3), 590–597.
[14] AND Z.L., BOWMAN R.S., *Counterion effects on the sorption of cationic surfactant and chromate on natural clinoptilolite*, Environ. Sci. Technol., 1997, 31 (8), 2407–2412.
[15] BAJDA T., KŁAPYTA Z., *Adsorption of chromate from aqueous solutions by HDTMA-modified clinoptilolite, glauconite and montmorillonite*, Appl. Clay Sci., 2013, 86 (3), 169–173.
[16] GOLESTANIFAR H., HAIBATI B., AMINI H., DEHGHANI M.H., ASADI A., *Removal of hexavalent chromium(VI) from aqueous solution by adsorption on alumina nanoparticles*, Environ. Prot. Eng., 2015, 41 (2), 133–145.
[17] ZHANG L., GAO Y., ZHOU Q., KAN J., WANG Y., *High-performance removal of phosphate from water by graphene nanosheets supported lanthanum hydroxide nanoparticles*, Water Air Soil Pollut., 2014, 225 (6), 1967.
[18] ZHANG L., WEI J., ZHAO X., LI F., JIANG F., *Competitive adsorption of strontium and cobalt onto tin antimonite*, Chem. Eng. J., 2016, 285, 679–689.
[19] SUN D., ZHANG X., WU Y., LIU X., *Adsorption of anionic dyes from aqueous solution on fly ash*, J. Hazard. Mater., 2010, 181 (1–3), 335–342.
[20] RATHORE V.K., DOHARE D.K., MONDAL P., *Competitive adsorption between arsenic and fluoride from binary mixture on chemically treated laterite*, J. Environ. Chem. Eng., 2016, 4 (2), 2417–2430.
[21] HOSSAIN M.A., NGO H.H., GUO W.S., NGHIEM L.D., HAI F.I., *Competitive adsorption of metals on cabbage waste from multi-metal solutions*, Bioresour. Technol., 2014, 160 (6), 79–88.
[22] HIDEKAZU T., SATOSHI F., ATSUSHI F., RYOZI H., TOMOKO K., *Microwave assisted two-step process for rapid synthesis of Na-A zeolite from coal fly ash*, Ind. Eng. Chem. Res., 2008, 47 (1), 226–230.
[23] SOMERSET V.S., PETRIK L.F., WHITE R.A., KLINK M.J., KEY D., *Alkaline hydrothermal zeolites synthesized from high SiO_2 and Al_2O_3 co-disposal fly ash filtrates*, Fuel, 2005, 84, 2324–2329.
[24] EIDEN-ASSMANN S., *New heavy metal-hydro-sodalites containing Cd^{2+}, Ag^{+} or Pb^{2+}: synthesis by ion exchange and characterization*, Mater. Res. Bull., 2002, 37 (5), 875–889.
[25] WANG Y.Q., ZHANG Z.B., LI Q., LIU Y.H., *Adsorption of uranium from aqueous solution using $HDTMA^{+}$-pillared bentonite: isotherm, kinetic and thermodynamic aspects*, J. Radioanal. Nucl. Chem., 2012, 293 (1), 231–239.
[26] ROUT P.R., BHUNIA P., DASH R.R., *Modeling isotherms, kinetics and understanding the mechanism of phosphate adsorption onto a solid waste: ground burnt patties*, J. Environ. Chem. Eng., 2014, 2 (3), 1331–1342.
[27] HYDER A.H.M.G., BEGUM S.A., EGIEBOR N.O., *Adsorption isotherm and kinetic studies of hexavalent chromium(VI) removal from aqueous solution onto bone char*, J. Environ. Chem. Eng., 2015, 3 (2), 1329–1336.

[28] NAMIN P.E., *Adsorption of copper, cobalt, and manganese ions from aqueous solutions using oxidized multi-walled carbon nanotubes*, Environ. Prot. Eng., 2016, 42, 75–85.
[29] KALIPCI E., *Removal of methylene blue from aqueous solutions with natural olive pomace*, Environ. Prot. Eng., 2016, 42 (3), 5–17.